Mine Water and the Environment (2024) 43:53–72
https://doi.org/10.1007/s10230-023-00968-w

TECHNICAL ARTICLE

Characteristics and Trend Prediction of Groundwater Chemical Evolution Under the Influence of Sea Water in the Jiaojia Gold Mining Area, China

Ying Wang[1] · Xia Wu[2] · Zhengqiu Liu[1] · Longqing Shi[3]

Received: 7 March 2023 / Accepted: 26 December 2023 / Published online: 10 February 2024

Abstract
Deep mining in the Jiaojia gold mine area has changed the chemical and flow characteristics of the groundwater there. We studied the relationship between the influent water sources and mine water, as well as the temporal and spatial distribution characteristics and evolution of groundwater chemistry using Piper diagrams, ion proportional coefficient analysis, and grey correlation analysis. The history and predicted groundwater chemical characteristics in the Jiaojia gold mine area were evaluated and a new method of researching the evolution of groundwater chemical characteristics was proposed that can more intuitively evaluate and predict vertical water sources. The main water inflow (inrush) source in the deep mine was shown to be water in the fractured fault footwall, followed by water in the fractured fault hanging wall. Due to mining, the hanging wall and footwall fractured aquifers now have a close hydraulic connection. As mining depth increases, permeability pathways between the seawater and mine water may be formed, causing higher concentrations of major ions near the Jiaojia fault zone and gold mines than in other areas.

Keywords Water filling sources · Chemical analysis of groundwater · Trends of hydrochemical evolution

Introduction

China has the fifth greatest gold reserves in the world and the greatest amount of mining. Due to the depletion of shallow gold resources, mining has gotten deeper, causing mine water inrush accidents to be common (Liu et al. 2022; Marion and Georg 2022). Since the mining of the Guilaizhuang gold deposit in Pingyi, Shandong Province, there have been 56 large and medium-sized water inrushes, of which the maximum water inrush was 2000 m^3/h, resulting in considerable economic losses (Zhang et al. 2021). These mine inrush accidents pose a serious threat to mining safety and production (Ou et al. 2013; Yao et al. 2012).

The Jiaojia gold deposit area is a metallogenic belt controlled by the Jiaojia fault in the Longkou Laizhou fault zone, and includes the Jiaojia, Xincheng, Sizhuang, and Wangershan gold deposits. In the shallow part of the mining area, the water inflow is very small, so there was little research on the water source and water inflow prediction. However, with deeper mining, the water inflow has increased every year. The water inflow increased from 4591 m^3/day in 2009 to 9483 m^3/day in 2018 in the Jiaojia gold mine; from 1225 m^3/day in 2011 to 1699 m^3/day in 2018 in the Xincheng gold mine; and from 4892 m^3/day in 2014 to 5629 m^3/day in 2018 in the Sizhuang gold mine.

Mine water inrush is usually determined by three factors water source(s), water-resisting layer(s), and water-conducting passageway(s) (Erdogan et al. 2019; Herrera et al. 2022). As the Jiaojia gold mine is close to the Bohai Sea (Paramaguru et al. 2021), with the increasing mining depth, deep seawater may, in the future, enter the mining area through the water diversion channel in the cataclastic rock on both sides of the fault, causing an

✉ Xia Wu
wx18764896712@163.com

[1] National Engineering Laboratory for Coalmine Backfilling Mining, Resource College, Shandong University of Science and Technology, Tai'an 271019, China

[2] Geophysical Prospecting and Surveying Team of Shandong Bureau of Coal Geology, Ji'nan 250104, China

[3] State Key Laboratory of Mining Disaster Prevention and Control Co-Founded by Shandong Province and the Ministry of Science and Technology, Shandong University of Science and Technology, Qingdao 266590, China

inrush. In addition, since the deep seawater is abundant, once a water-conducting passageway forms, it will pose a great threat to safe mining. Therefore, studying the deep hydrochemical evolution characteristics and predicting its evolution trend under the influence of seawater in the Jiaojia gold mine area can provide a theoretical basis for the research of water control theory and technology of deep gold mines (Luo et al. 2022; Subodh et al. 2022; Sunkari et al. 2022; Weightman et al. 2020), and will have a practical mine safety application (Arefieva et al. 2019; Tarasenko et al. 2022; Zhang et al. 2021).

Study Area

Geological Characteristics

The Jiaojia gold mine area strata are relatively simple the Cenozoic Quaternary is distributed in the northwestern portion of the area, and the Archaean and Proterozoic Jiaodong group (Ar-Ptljf) is located in the southwestern part, in the upper wall of the Jiaojia fault zone and in the biotite granite (γ_5^1). The Jiaodong group (Ar-Ptljf) strata have intrusive contact or fault contact with the Mesozoic magmatic rocks (Fig. 1). The Quaternary (Q) strata is mainly composed of sandy clay rock, pebbly sandy clay rock, and

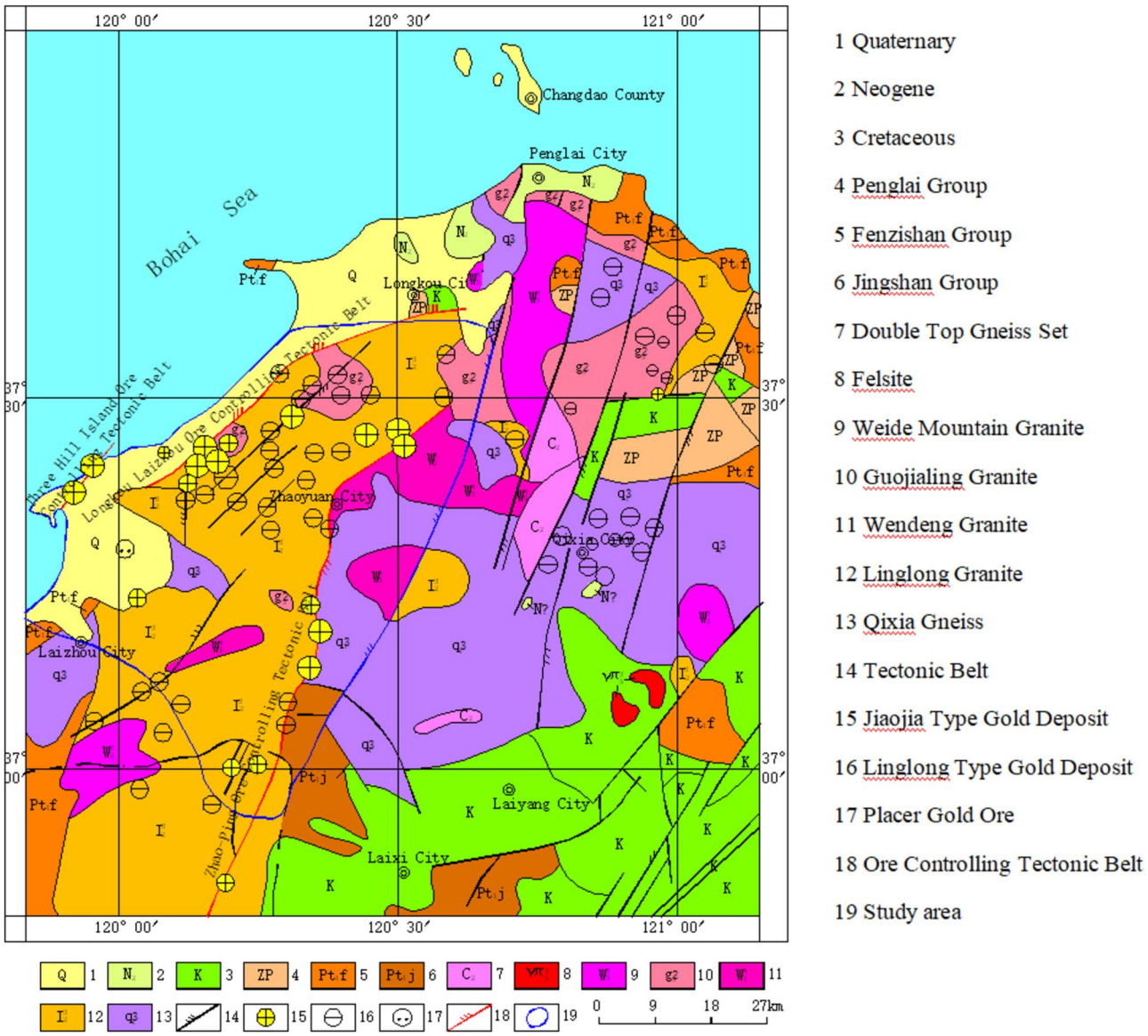

Fig. 1 Northwest regional geological map of Jiaojia

sand and gravel, while the Jiaodong group (Ar-Ptljf) are composed of banded migmatite plagioclase amphibole, with a banded and mottled structure.

The Archean Paleoproterozoic metamorphic basement rock series is widely distributed in the area and is the gold-bearing formation. Tectonic activity and magmatic intrusions were the heat source that activated the gold-bearing fluids. Since the Mesozoic, brittle faults have developed with different directions and orders, mainly in the NNE and NE directions, providing channels and spaces for the migration and enrichment of the gold deposits.

The main magmatic rocks in the study area are granodiorite and biotite granite. The granodiorite (γ_5^2) in the study area occurs in the footwall of the Jiaojia fault zone and has a magmatic origin based on its texture, structure, flow structure, and sulfur isotope ratio. It is 50–100 m wide and 1900 m in length. It is light gray to grayish white in color, with a porphyritic-like texture; the matrix has a hypautomorphic granular texture. The gold deposits are mostly located in the top contact zone of the internal and external rock mass and were deposited in the post-magmatic period after the rock mass formed and before the mafic dikes formed.

The biotite granite (γ_5^1) is widely distributed in the study area and is mainly distributed in the hanging wall of the Jiaojia fault and the eastern part of the mining area. It is in intrusive contact with the Jiaodong group strata and shows a local harmonious transition relationship.

Structural Features

The Jiaojia Fault Zone

The Jiaojia fault zone is more than 20 km long and 100–200 m wide, with an average strike of 40°; the tendency is northwest and the dip angle is 20°–30° with locally steeper locations, up to 70° (Fig. 2). The fault zone is a wide crush zone composed of cataclastic and granitic cataclastic rocks, and there is a grey-black and gray-white fault gouge that is 10–20 cm thick. The local occurrence of small folds along the fault zone shows the properties of the compressional torsion fracture. Variably thick and discontinuous mylonite and breccia occur along the fault zone. The cataclastic and granitic cataclastic rocks are bended and symmetrically distributed in the hanging wall and footwall of the main fault,

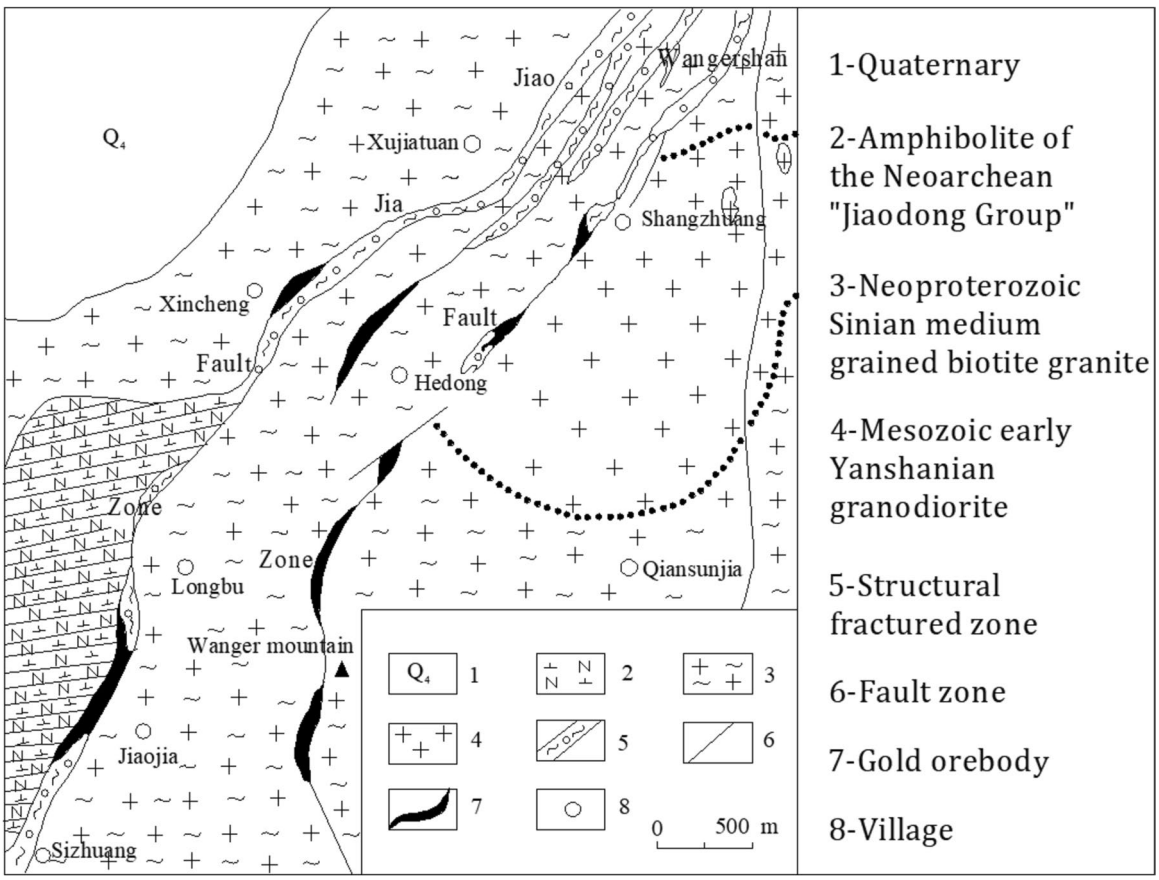

Fig. 2 Distribution of gold deposits in Jiaojia fault zone and its branches

but the gold ores usually occur in the footwall of the main fault, where the hydrothermal liquid mineralization caused alteration and mineralization (Table 1).

The Wangershan Fault Zone

The Wangershan fault zone is 13 km long and 20–120 m wide; the average strike is 40º, the tendency is northwest, and the dip angle ranges from 45º to 60º. The characteristics of the tectonic rock in the Wangershan fault zone are consistent with that in Jiaojia fault zone, with only slight differences in degree of development and scale. The Wangershan fault zone is also a compression torsion fault and belongs to a secondary fault structure that is derived from the Jiaojia fault zone.

Hydrogeological Characteristics

The ore-controlling structure of the Jiaojia gold mine area is the Jiaojia fault zone, which is adjacent to the Bohai Sea in the north and Laizhou Bay in the northwest. Considering the water storage mode, groundwater hydraulic characteristics, water abundance, location of each rock layer, and their effect on the mining of the deposit, the strata are divided into six categories the Quaternary alluvial aquifer, the fractured weathered bedrock aquifer, fractured fault hanging wall aquifer, intermediate aquifuge, fractured fault footwall aquifer, and floor aquifuge (Fig. 3).

The Quaternary alluvial aquifer is the shallowest layer of the deposit, with a thickness of 4 ~ 28 m. It is relatively thick locally due to the influence of the terrain. The lithology changes greatly, and there is a 0.5 ~ 1.0 m gravel layer at the bottom with good permeability, which allows the underlying fractured weathered bedrock aquifer to be recharged by atmospheric precipitation.

The fractured weathered bedrock aquifer is distributed over the entire deposit and under the Quaternary strata, with a general thickness of 20 ~ 45 m. The lithology is composed of monzonitic granite in the northwest and metagabbro in the hanging wall of the Jiaojia main fault, with moderate to strong water abundance. Under tectonic movement and weathering, the rock developed cracks, so the permeability coefficient is 0.1 ~ 1.0 m/d and the specific well discharge is 0.1 ~ 0.5 L/s m. Most of the monzonitic granite aquifers in

Table 1 Zonation and lithology of rock in the Jiaojia fault zone

Hanging wall and footwall	Zonation and characteristics of tectonic rocks in ore bearing areas				
	Name	Intensity of mineralization	Texture and structure	Alteration characteristic	Mineralization characteristic
Hanging wall of Jiaojia fault zone	Biotite granite	Non-industrial mineralization			
	Phyllic granite		Palimpsest cataclastic granite texture, massive structure	Weak sericitization, silicification and scattere dpyritization	Scattered mineralization
	Phyllic granitic cataclstic rock		Palimpsest cataclastic granite texture, massive structure, taxitic structure		
	Phyllic calaclastic rock		Palimpsest cataclastic texture, taxitic structure		
	Fault gouge			Weak	
Footwall of Jiaojia fault zone	Beresite	Industry ore bodies	Palimpsest mylonitic texture, banded structure	Beresitization successive reduced	Disseminated mineralization
	Beresitizatic cataclstic rock		Palimpsest cataclastic texture, taxitic texture		Mottled and short vein mineralization
	Beresitizatic granodioritic cataclstic rock		Palimpsest cataclastic texture, taxitic texture, mesh-vein structure		Fine vein disseminated mineralization
	Beresitizatic or phyllic granodiorite		Palimpsest cataclastic texture, massive structure, mesh-vein structure		Mesh-vein mineralization
	Granodiorite				Scattered mineralization

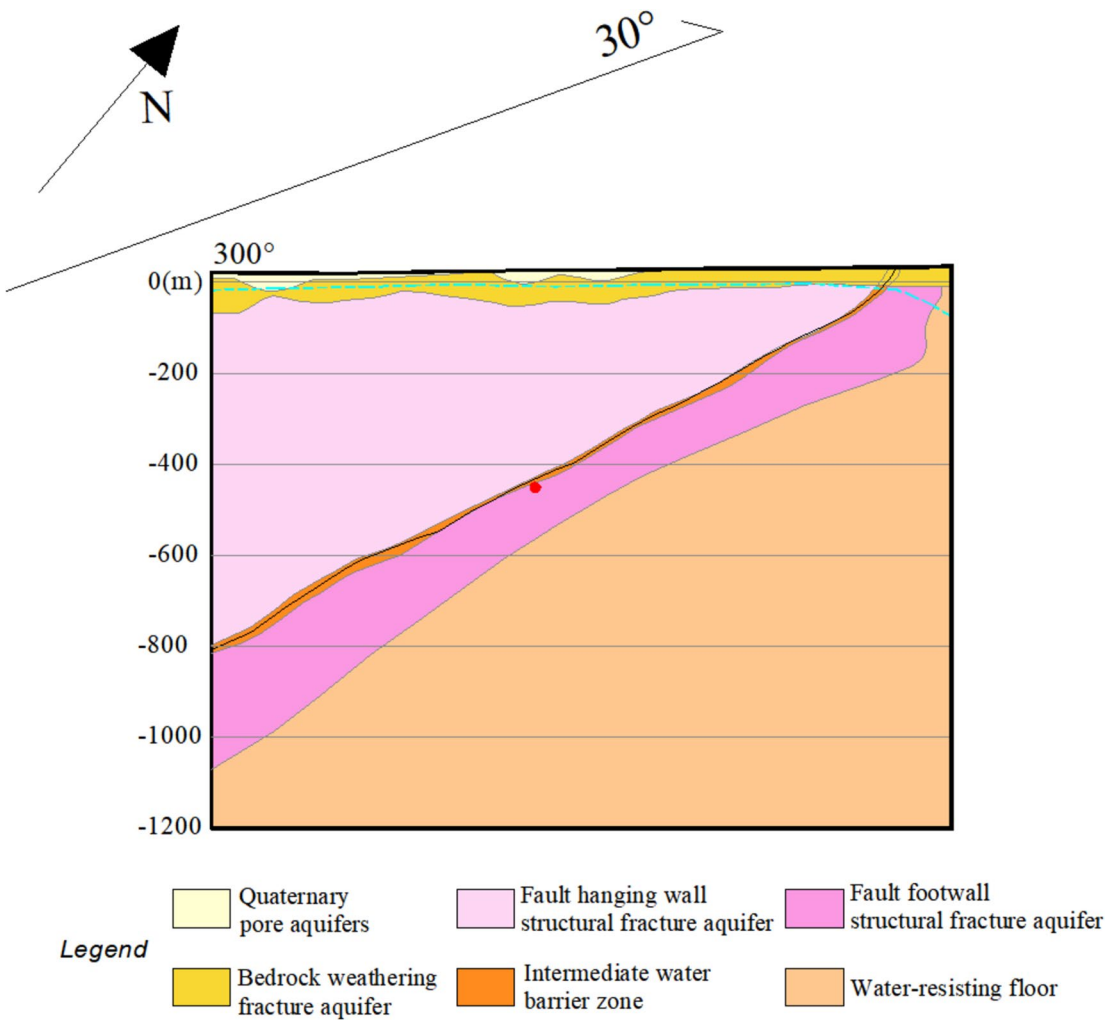

Fig. 3 Hydrogeological profile of Jiaojia gold deposit

the northwest are directly exposed to the surface, containing vein fissure water, with poor fissure development, permeability coefficient of 0.1 ~ 3.0 m/d, and the specific well discharge of less than 0.1 L/s m. They are weakly water-rich aquifers.

The fractured fault hanging wall aquifer is located in the hanging wall of the Jiaojia main fault. It is composed of granitic cataclasite, metagabbro, metagabbro cataclasite, etc. The thickness varies greatly and increases from the Jiaojia main fault to the west, and mainly contains structural fracture water, with uneven water abundance and permeability. The fractures are relatively developed, but most of them are compressive torsional and torsional fractures, with poor water conductivity. The permeability coefficient is 0.001 ~ 0.1 m/d and the specific well discharge is 0.004 ~ 0.098 L/s m, with weak water abundance and permeability. The weathered bedrock fracture aquifer mainly recharges it, and its bottom boundary is the intermediate aquifuge represented by the fault gouge. Since the ore body mainly occurs in the fault footwall, the water in the fractured fault hanging wall is the indirect water-filling aquifer, which can only be transformed into a direct water-filling aquifer when the mining engineering destroys the intermediate aquifuge.

The intermediate aquifuge is mainly composed of altered pyrite cataclasite and dark gray fault gouge, is continuously distributed, and has good impermeability. It is located in the middle of Jiaojia main fault zone, with a strike of 12°, a dip angle of 25° ~ 45°, a NW tendency, and an extension of more than 1000 m. The fractured fault footwall aquifer is located in the footwall of Jiaojia main fault and is mainly composed of altered pyrite granite cataclasite and altered pyritic granite. The aquifer is distributed along the bottom of the intermediate aquifuge, with a thickness of 22–305 m. The permeability coefficient is 0.002 ~ 0.75 m/d, and the specific well discharge is 0.001 ~ 0.1 L/s m, with weak to moderate water abundance. The ore body and mining system are mainly located in this aquifer, and it is the direct water-filling source of the deposit.

The floor aquifuge is located under the fractured fault footwall aquifer and is mainly composed of monzogranite. The fractured fault footwall aquifers cover the vicinity of the main fault, while the Quaternary alluvial aquifers and weathered fractured bedrock aquifers mainly cover the east side. The floor aquifuge is more than 1000 m thick. Its fractures are underdeveloped, so it is an anhydrous rock mass with poor water abundance and permeability.

Hydrochemical Characteristics Analysis

368 samples (Fig. 4) were collected from January 1968 to December 2021 in the Jiaojia mine area (Table 2), including 77 water samples of Quaternary alluvial aquifer, 148 water samples of weathered fractured bedrock aquifer, 67 water samples of fractured fault hanging wall aquifer, 47 fractured fault footwall aquifer water samples, and 29 samples of mine water. Among the mine water samples were two water inrush points in the Jiaojia gold mine roadway, j2013-330 and j2013-630. The conventional ions mainly include $K^+ + Na^+$ (due to the low content of K + and its similar chemical

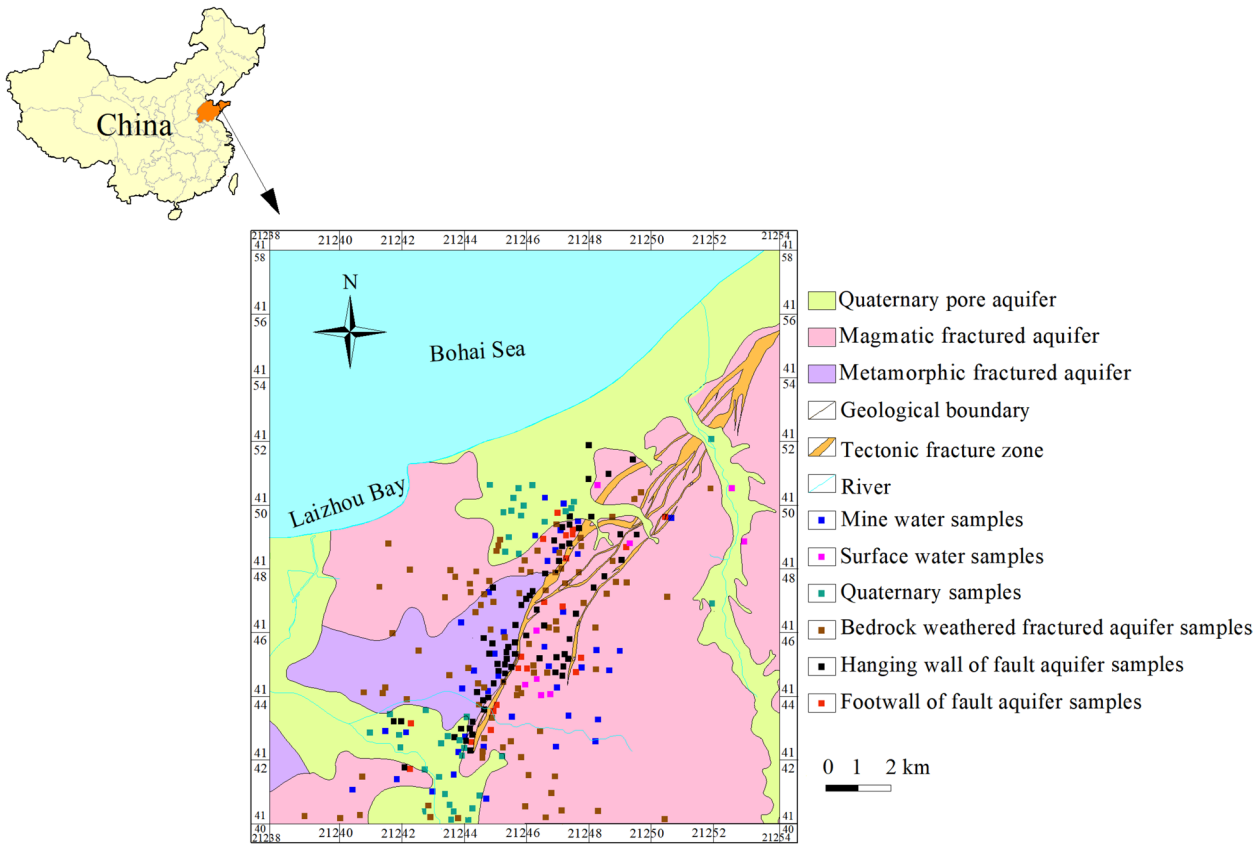

Fig. 4 Location of Jiaojia gold mine area and distribution of groundwater sampling points

Table 2 Number of water samples per year

1968	1969	1970	1971	1972	1973	1974	1975	1976	1977	1978	1979	1980	1981	1982	1983	1984	1985
1	2	1	2	3	2	1	3	2	3	2	1	3	2	1	3	1	2
1986	1987	1988	1989	1990	1991	1992	1993	1994	1995	1996	1997	1998	1999	2000	2001	2002	2003
2	3	4	5	3	2	6	4	5	2	4	3	2	4	3	2	3	5
2004	2005	2006	2007	2008	2009	2010	2011	2012	2013	2014	2015	2016	2017	2018	2019	2020	2021
3	4	6	5	4	6	4	6	12	32	56	38	72	4	5	4	6	4

properties with Na+, Na+was used instead), Ca^{2+}, Mg^{2+}, Cl^{-}, $SO4^{2-}$, HCO_3^{-}, CO_3^{2-}, and TDS (Chen et al. 2021; Khy et al. 2018; Krzysztof et al. 2021).

Analytical Method

We drew the Piper and Durov diagram using AQ–QA software, which is a powerful and easy-to-use tool for hydrological data analysis (Swa et al. 2021). It helps users analyze and interpret hydrological data, import and process various hydrochemical data, and provides image display and data analysis functions to support hydrogeochemistry research. Using Surfer 17 software, we drew the contour map of each aquifer's primary ion proportion coefficient using the Kriging interpolation method. The Kriging interpolation can give appropriate weight to the measured values around to get the predicted value of an unmeasured position. The commonly used formula of its interpolator is composed of the weighted sum of the data

$$\hat{Z}(s_0) = \sum_{i=1}^{N} \lambda_i Z(s_i) \quad (1)$$

where $Z(s_i)$ is the measured value at position i; λ_i is the unknown weight of the measured value at position i; s_0 is the predicted position; and N is the number of measurements. The weight λ_i depends not only on the distance between the measurement points and the predicted position, but also on the overall spatial arrangement based on the measurement points. Therefore, the weight λ_i depends on the distance between the measuring point and predicted position, and the fitting of the spatial relationship between the measured values around the predicted location.

We drew the line diagram of the main ion proportion coefficient as the water of each aquifer changed with time using Origin 9.1 software, which supports a variety of 2D/3D diagram. The curve was fitted by the nonlinear least square method based on the Levernberg-Marquardt algorithm.

Analysis of the Piper Diagram

Aq·QA software enables one to more intuitively observe and analyze the hydrochemical characteristics of water samples from different aquifers and the relationship between them. The Piper diagram consists of two triangles and a diamond. The three edges of the lower left triangle represent the milligram equivalent percentages of cations $Na^+ + K^+$, Ca^{2+}, and Mg^{2+}. The lower right triangle represents the milligram equivalent percentage of anions Cl^-, SO_4^{2-}, and $HCO_3^- + CO_3^-$. The relative content of anions and cations in any water sample is represented by the positions marked in the two triangles respectively, and the crossover point obtained by the diamond is a comprehensive representation of the relative content of anions and cations in this water sample. The long edge of the rectangle on the right side of the Durov diagram represents the size of TDS data.

189 mine water samples and mine water filling source samples were collected from 2014 to 2021. As time passed, the color corresponding to the mark of each water sample changed from light to dark (Fig. 5). The Ca^{2+}, Mg^{2+}, and SO_4^{2-} concentrations in the Quaternary alluvial water increased, while the HCO_3^- concentration decreased. The hydrochemical facies evolved from Cl-Na·Ca to HCO_3·SO_4·Cl-Ca type. The Na^+, Ca^{2+}, and Cl^- concentrations in the fractured weathered bedrock water increased, while the SO_4^{2-} and HCO_3^- concentrations decreased. The hydrochemical facies evolved from HCO_3-Ca to HCO_3·SO_4·Cl-Ca type. The Ca^{2+}, SO_4^{2-}, and HCO_3^- concentrations of water in the fractured fault hanging wall increased, while the Na^+ concentration decreased. The hydrochemical facies evolved from HCO_3·Cl-Na·Ca to HCO_3·SO_4·Cl-Ca type. The Ca^{2+} and Cl^- concentrations in the fractured fault footwall's water increased, while the Na^+ and HCO_3^- concentrations decreased. The hydrochemical facies evolved from HCO_3·Cl-Ca to HCO_3·SO_4·Cl-Ca type. The Na^+ and Cl^- concentrations in the mine water increased, while the Ca^{2+} and HCO_3^- concentrations decreased. The hydrochemical facies evolved from HCO_3-Ca to Cl-Na type (Fig. 5). The EC value of the Quaternary alluvial water, weathered fractured bedrock water, fractured fault hanging wall water, fractured fault footwall weathered fractured, and mine water were 768, 1016, 2139, 3120, and 3118, respectively.

The hydrochemical type of the seawater is similar to the water in the fractured fault footwall and mine water, followed by water in the fractured fault hanging wall, and different from the fractured weathered bedrock water and Quaternary alluvial water. As mining proceeded, the Na^+ and Ca^{2+} concentrations in the Quaternary alluvial water and bedrock weathering fracture water have decreased, while the Mg^{2+} concentration changed little, indicating consistent cation exchange reactions. The Na^+ concentration in the water of the fractured fault hanging wall and footwall increased, while the Ca^+ and Mg^{2+} concentration slightly decreased, indicating a strong cation exchange reaction. The Cl^- concentration in the water of each aquifer increased and the groundwater became more saline (Fig. 5).

Analysis of the Proportional Coefficient

Spatial Distribution of the Ion Proportional Coefficient

189 samples were selected from 2014 to 2021 37 Quaternary alluvial water samples, 99 fractured weathered bedrock water samples, 22 fault hanging wall structural fracture

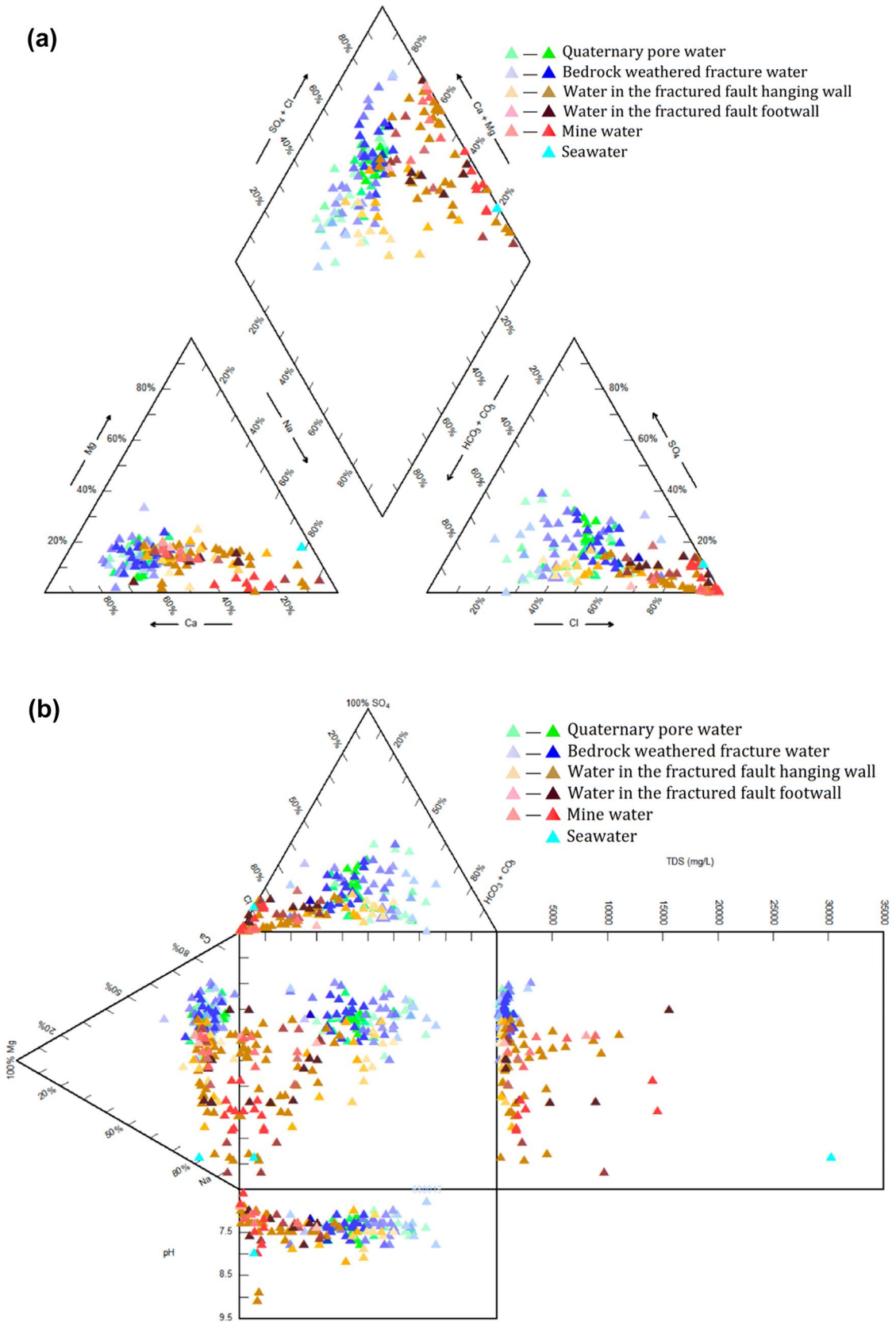

Fig. 5 Piper and Durov diagram of water sample of water filling sources and the water inflow point; **a** Piper diagram; **b** Durov diagram

water samples, 22 fractured fault footwall water samples, and 9 mine water samples.

Except for the sodium adsorption ration (SAR), the average values of other ion proportion coefficients of the Quaternary alluvial water were the largest, and the water in the fractured fault footwall were the smallest (Table 3). Table 4 and Fig. 6 show that all of the samples had γNa/γCl values less than 1.0, indicating that the mine water was not affected by the leaching of atmospheric precipitation. The γNa/γCl values of other samples were less than 0.85, indicating that ion exchange had occurred, increasing the Ca^{2+} content and decreasing the Na^{+} content. The increased γNa/γCl value indicates that the intensity of salt leaching and its accumulation had increased. The γCa/γCl value of all samples were less than 1, indicating poor groundwater dynamic conditions. The value of $\gamma SO_4/\gamma Cl$ was less than 1, which indicates that Cl^{-} in the mine water increased faster than SO_4^{2-}; the value of $\gamma HCO_3/\gamma Cl$ was less than 0.1, indicating that the water quality became more saline. The SAR value of the S160502 sample was the highest, indicating

Table 3 Statistics of ion proportional coefficient characteristic of water samples

Ion proportional coefficient	Quaternary alluvial water			Bedrock weathered fracture water			Water in the fractured fault hanging wall		
	Maximum value	Minimum value	Mean value	Maximum value	Minimum value	Mean value	Maximum value	Minimum value	Mean value
$\frac{\gamma Na}{\gamma Cl}$	1.92	0.22	0.76	2.07	0.15	0.69	1.25	0.07	0.62
$\frac{\gamma Ca}{\gamma Na}$	23.46	0.05	2.5	5.83	0.29	2.35	12.3	0.11	1.59
$\frac{\gamma Mg}{\gamma Na}$	11.03	0.09	0.7	2.09	0.08	0.61	0	5.6	0.52
$\frac{\gamma Ca}{\gamma Cl}$	5.26	0.08	1.64	4.43	0.2	1.46	1.73	0.05	0.72
$\frac{\gamma SO_4}{\gamma Cl}$	3.31	0	0.53	3.78	0	0.47	0.79	0	0.13
$\frac{\gamma HCO_3}{\gamma Cl}$	6.86	0.09	1.1	5.26	0.03	0.91	1.94	0	0.48
SAR	7.9	0.1	1.84	9.1	0.61	1.93	29.73	0.2	4.83

Ion proportional coefficient	Water in the fractured fault footwall			Mine water		
	Maximum value	Minimum value	Average values	Maximum value	Minimum value	Average values
$\frac{\gamma Na}{\gamma Cl}$	1.37	0.11	0.62	0.87	0.45	0.69
$\frac{\gamma Ca}{\gamma Na}$	2.63	0.05	1.05	1.02	0.28	0.52
$\frac{\gamma Mg}{\gamma Na}$	7	0.06	0.5	0.33	0.46	0.09
$\frac{\gamma Ca}{\gamma Cl}$	0.89	0.05	0.53	0.46	0.25	0.33
$\frac{\gamma SO_4}{\gamma Cl}$	0.52	0	0.11	0.13	0.01	0.08
$\frac{\gamma HCO_3}{\gamma Cl}$	0.91	0.01	0.25	0.07	0.004	0.04
SAR	51.77	0.88	7.3	6.2	1.48	4

Tips: γ is the milligram equivalent concentration of ions, meq/L; SAR is the sodium adsorption ratio, where $SAR = \frac{Na^{+}}{\sqrt{\frac{1}{2}(Ca^{2+}+Mg^{2+})}}$, and C is the concentration, meq/L

Table 4 Statistical of ion proportional coefficient of mine water in the Jiaojia gold mine area

Number	Sample ID	Sampling location	$\frac{\gamma Na}{\gamma Cl}$	$\frac{\gamma Ca}{\gamma Na}$	$\frac{\gamma Mg}{\gamma Na}$	$\frac{\gamma Ca}{\gamma Cl}$	$\frac{\gamma SO_4}{\gamma Cl}$	$\frac{\gamma HCO_3}{\gamma Cl}$	SAR
1	S160501	Exploration roadway 1# of Xincheng gold mine	0.856	0.300	0.028	0.257	0.129	0.059	6.105
2	S160502	Exploration roadway 2# of Xincheng gold mine	0.869	0.283	0.040	0.246	0.120	0.061	6.199
3	S160508	Middle section of – 630 m in Sizhuang gold mine	0.670	0.453	0.023	0.303	0.022	0.009	4.207
4	S160509	Middle section of – 630 m in Wangershan gold mine	0.723	0.442	0.056	0.319	0.063	0.039	4.016
5	S1610580	Middle section of – 630 m in Xincheng gold mine	0.670	0.527	0.094	0.353	0.120	0.023	3.222
6	S1610581	– 630 m observation point of Xincheng gold mine	0.757	0.377	0.094	0.286	0.125	0.044	4.244
7	J2013-630	Water inrush point of – 630 m roadway in Jiaojia gold mine	0.561	0.731	0.053	0.410	0.007	0.004	2.552
8	J2013-330	Water inrush point of – 330 m roadway in Jiaojia gold mine	0.447	1.024	0.330	0.458	0.016	0.074	1.477
9	S210701	Middle section of – 650 m in Jiaojia gold mine	0.613	0.623	0.032	0.296	0.012	0.011	2.932

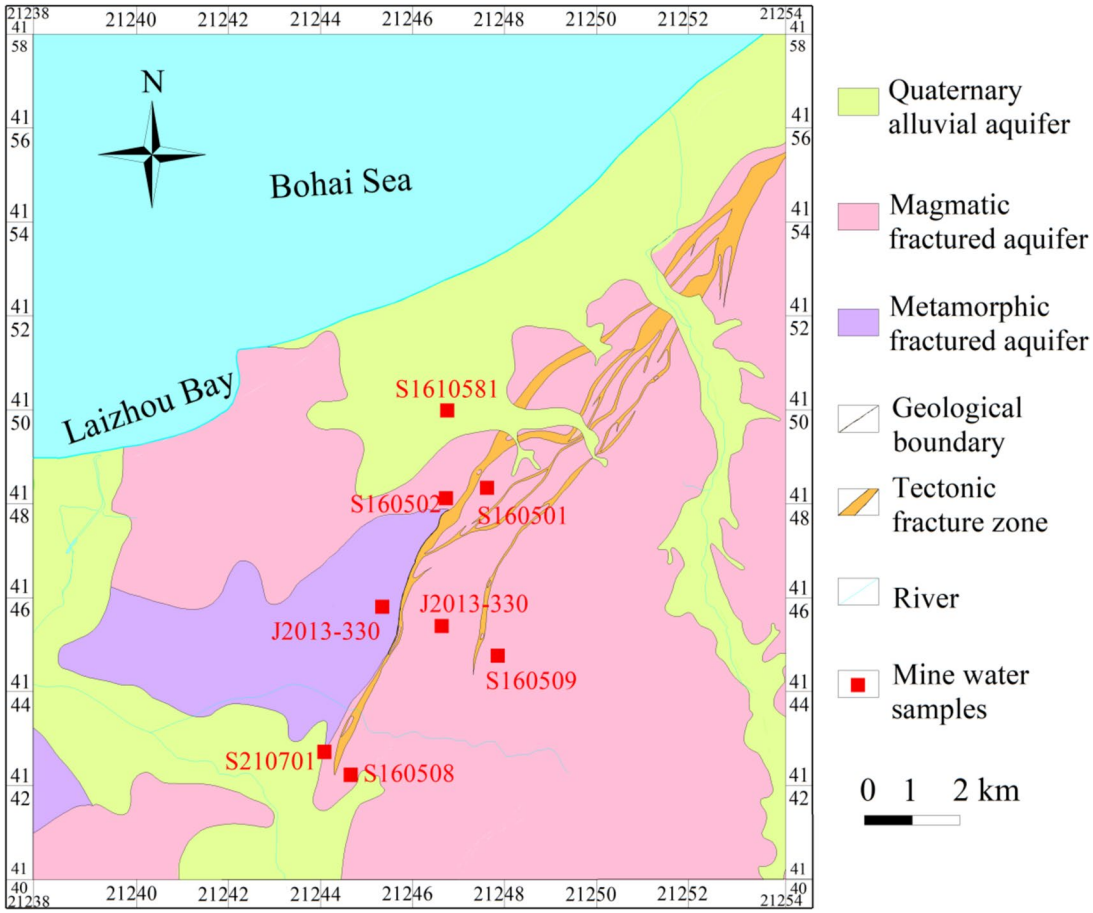

Fig. 6 Distribution of mine water sampling location

that the sample contained abundant exchangeable Na^+. The SAR value increased with the mining depth and the cation exchange intensity increased between Ca^{2+}, Mg^{2+} (groundwater), and Na^{2+}(rock). The SAR value of the J2013-330 sample was less than 2, indicating no seawater intrusion, while the rest exceeded 2, indicating that they may have been affected by seawater.

Almost all of the γCa/γCl values exceeded 1, indicating good dynamic conditions of the Quaternary aquifer (Fig. 7b). They exceeded 2 in the southwest area, which may be because rock fractures are developed in the lower part of the Quaternary alluvial aquifer close to the Jiaojia fault zone. The γCa/γCl value in the southeast exceeded 2, possibly due to its location in the mountains, large surface drop, and good hydrodynamic conditions. The $\gamma SO_4/\gamma Cl$ value near the Sizhuang gold mine was less than 1 (Fig. 7c), which potentially mean it is related to seawater. The SAR value exceeded 2 in Sizhuang and the coastal area (Fig. 7d), indicating strong water–rock interaction.

The contour map of the ion proportion coefficient in the fractured bedrock aquifer shows that an area with a γNa/γCl value close to 0.85 was distributed in the southwest near the Jiaojia fault and along the coast of Laizhou Bay (Fig. 8a), indicating this groundwater is related to seawater. The γCa/γCl value in most areas was less than 1 (Fig. 8b), indicating poor hydrodynamic conditions. The γCa/γCl value near the Jiaojia fault in the southwest and the southeast of Sizhuang exceeded 1, indicating a good hydrodynamic condition, which may be due to the development of fractures and good permeability near the Jiaojia fault zone. The $\gamma SO_4/\gamma Cl$ value of most areas was less than 1 (Fig. 8c), potentially indicating seawater intrusion. In the northeast of the Jiaojia fault zone and near the Jiaojia gold mine, the SAR value reaches 7 or more (Fig. 8d), indicating the intensity of the cation exchange reaction between water and rock.

The contour map of the ion proportion coefficient in the fractured fault hanging wall aquifer shows that an area with a γNa/γCl value close to 0.85 was distributed near and southwest of the Jiaojia fault (Fig. 9a), in the Jiaojia and Sizhuang gold mines. The γNa/γCl value near and west of the Jiaojia gold mine and the south-north section of the Jiaojia fault zone is close to 1, the salt was enriched, which may be due to the leaching of saline rock strata. The γNa/γCl values in the northeast were less than 0.85, indicating that ion exchange

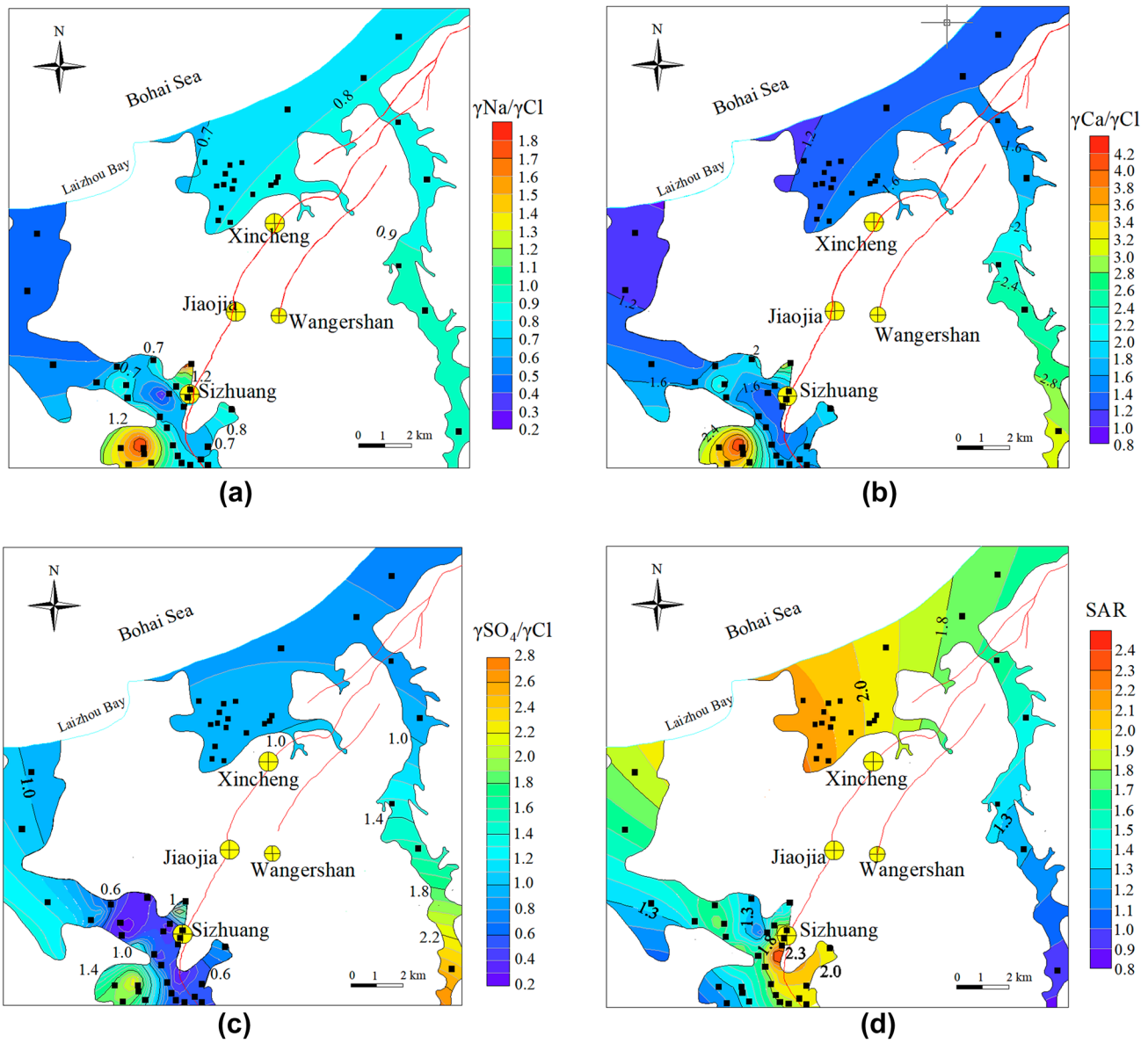

Fig. 7 Contour map of ion proportion coefficient of the Quaternary alluvial water **a** γNa/γCl; **b** γCa/γCl; **c** $\gamma SO_4/\gamma Cl$; **d** SAR

had occurred, increasing the Ca^{2+} content and decreasing the Na^+ content. The area with a γCa/γCl value exceeding 1 was concentrated in the west of the middle and south sections of the Jiaojia fault zone (Fig. 9b), indicating a good hydrodynamic condition. This may be due to the opening of fractures and the formation of water-conducting passageways during mining. The area's overall $\gamma SO_4/\gamma Cl$ value was less than 1 (Fig. 9), potentially indicating seawater intrusion. In most areas, the SAR value exceeded 2, and the SAR value reached 10 or more near the south-north part of the Jiaojia fault zone (Fig. 9d), indicating a strong cation exchange reaction between water and rocks.

The contour map of the ion proportion coefficient in the fractured fault footwall aquifer shows that an area with a γNa/γCl value close to 0.85 was distributed in the South–North section of the Jiaojia fault zone (Fig. 10a). The γNa/γCl value near the Sizhuang gold mine was close to 1, and the salt is enriched, which could be due to dissolution of saline rock strata. The γNa/γCl value elsewhere was less than 0.85, indicating that ion exchange had occurred, increasing the Ca^{2+} content and decreasing the Na^+ content. The area's overall γCa/γCl value was less than 1, indicating a poor hydrodynamic condition. The γCa/γCl values of the western Sizhuang gold mine and the Xincheng gold mine were close to 1 (Fig. 10b), with good dynamic conditions. The area's overall $\gamma SO_4/\gamma Cl$ value was less than 1 (Fig. 10c), indicating that the water quality is becoming more saline. The SAR value reached 8 or more southwest of the Sizhuang

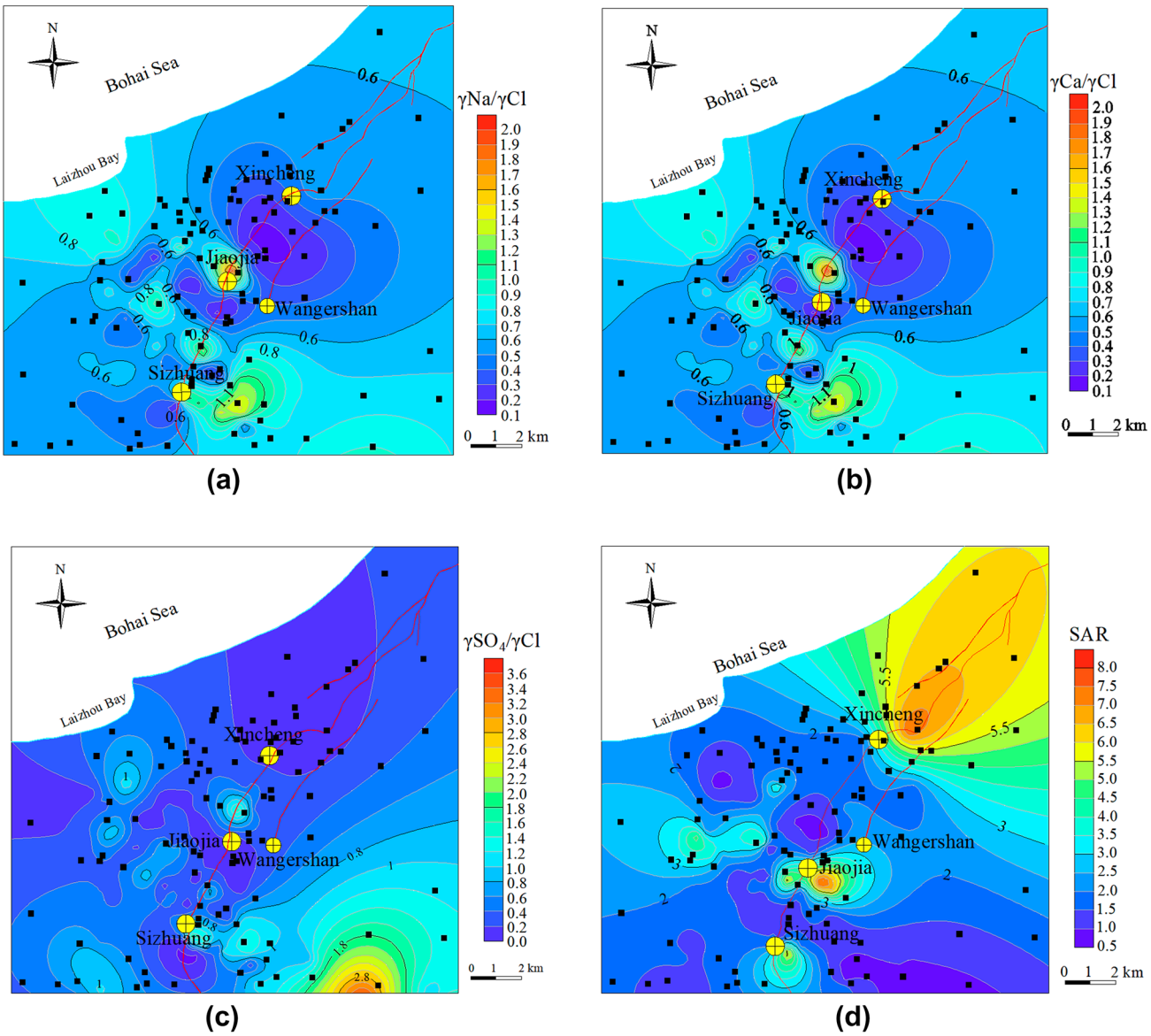

Fig. 8 Contour map of ion proportion coefficient of the bedrock weathering fractured water **a** γNa/γCl; **b** γCa/γCl; **c** γSO4/γCl; **d** SAR

gold mine, and the maximum value was 51.77 (Fig. 10d), indicating a strong cation exchange reaction between water and rock.

Time Distribution of the Ion Proportional Coefficient

From 1968 to 2020, 50 samples of Quaternary alluvial water, 102 samples of bedrock weathered fracture water, 58 samples of fractured fault hanging wall water, 36 samples of water in the fractured fault footwall, and 30 samples of mine water were collected from the Jiaojia gold mine area, with 3 year sampling periods. Due to the spatial variation of the Jiaojia fault zone and the ore body's location, the sampling depth of the fractured fault hanging wall water samples increased as the mining depth increased.

The average Na^+, Cl^-, SO_4^{2-}, EC, γNa/γCl, γCa/γCl, $\gamma SO_4/\gamma Cl$, and SAR values for each time interval of each aquifer were calculated to analyze the relationship between aquifers by the change of dynamic hydrochemical characteristics. Figure 11 shows that the Na^+ concentration of the Quaternary alluvial water and the fractured bedrock water changed little with the increased mining depth; both basically kept below 200 mg/L with solid correlation, indicating a close hydraulic connection. The Na^+ concentration in the fractured fault hanging wall water increased slightly, while the mine water and the water in the fractured fault footwall increased greatly, reaching 1000 mg/L or more. The rising

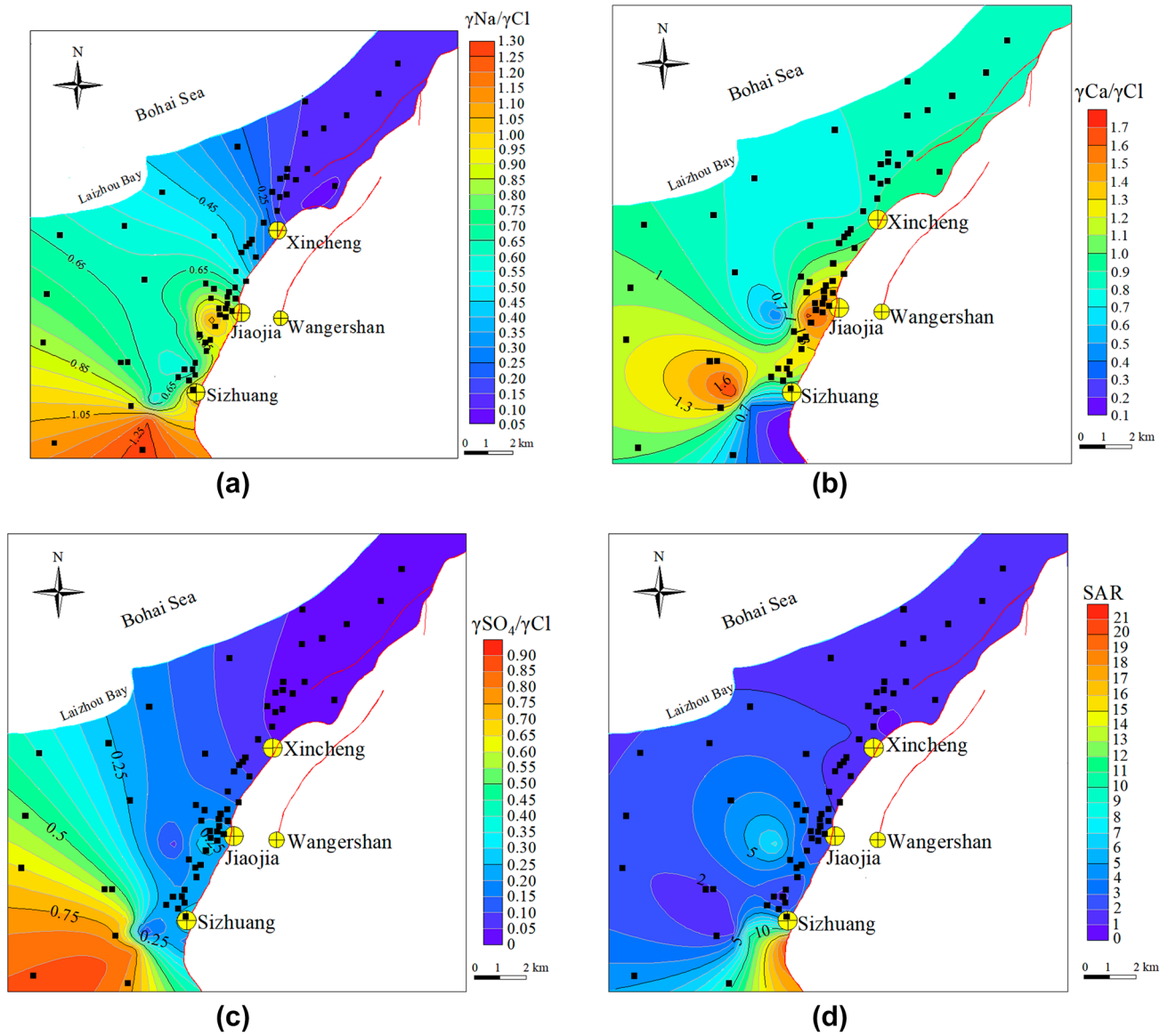

Fig. 9 Contour map of ion proportion coefficient of the water in the fractured fault hanging wall **a** γNa/γCl; **b** γCa/γCl; **c** γSO4/γCl; **d** SAR

trends have a strong correlation, indicating that the mine water mainly comes from the fractured fault footwall water.

Figure 12 shows that the Cl^- concentration of the Quaternary alluvial water changed little with increased mining depth and basically remained below 300 mg/L, while it increased slightly in the weathered fractured bedrock water. The Cl^- concentration of the water in the fractured fault hanging wall, in the fractured fault footwall and the mine water increased greatly, reaching 3000 mg/L or more. The Cl^-concentration of the water in the fractured fault footwall and the mine water had an increasing trend, which may be related to seawater.

Figure 13 shows that with the increased mining depth, the SO_4^{2-} concentration of the Quaternary alluvial water, the weathered fractured bedrock water, the water in the fractured fault hanging wall, and the mine water increased to a certain extent, finally reaching 150 mg/L. The SO_4^{2-} water concentration in the fractured fault footwall increased greatly, which may be related to the seawater.

Figure 14 shows that with the increased mining depth, the EC changed little in the Quaternary alluvial water, increased in the weathered fractured bedrock and fractured fault hanging wall water, and increased greatly in the fractured fault footwall water, indicating the soluble salt content increased with depth, and that the water in the fractured fault hanging wall and footwall are closely related to the mine water.

Figure 15 shows that with the increased mining depth, the $\gamma SO_4/\gamma Cl$ value of Quaternary alluvial water and bedrock

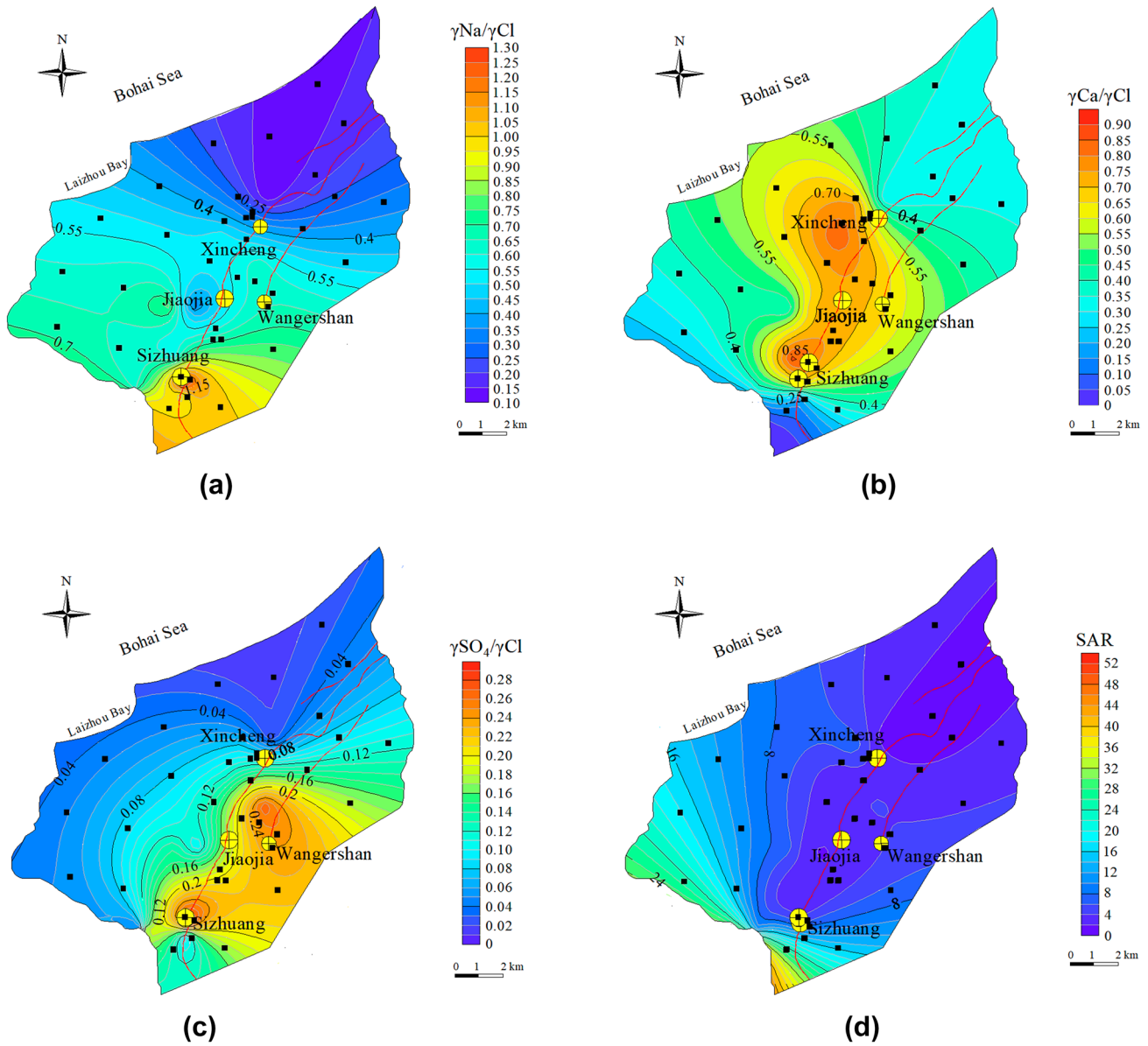

Fig. 10 Contour map of ion proportion coefficient of the water in the fractured fault footwall **a** γNa/γCl; **b** γCa/γCl; **c** γSO4/γCl; **d** SAR

fracture water increased as the Cl^- increased slowly. The $\gamma SO_4/\gamma Cl$ values of the water in the fractured fault hanging wall and footwall was unchanged, and finally approached 0.1, which is far less than 1, indicating that Cl^- increased rapidly and that seawater was intruding. The $\gamma SO_4/\gamma Cl$ value of the mine water changed greatly, and in the rear section was similar to the $\gamma SO_4/\gamma Cl$ value of the water in the fractured fault hanging wall and footwall, indicating a close relationship. The $\gamma SO_4/\gamma Cl$ value of the water in the fractured fault hanging wall and footwall approached that of the seawater.

Figure 16 shows that with the increased mining depth, the SAR values of the Quaternary alluvial water and fractured bedrock water remain unchanged, indicating the intensity of cation exchange reaction changed little. Some SAR values exceeded 2, indicating possible seawater intrusions. The SAR values of the water in the fractured fault hanging wall and footwall increased, indicating an increased intensity of exchange reaction changes and strong water–rock interaction. The SAR value of the mine water increased, consistent with the water trend in the fractured fault footwall, indicating a close relationship between the two. The SAR value of the mine water in the later section was close to the water in the fractured

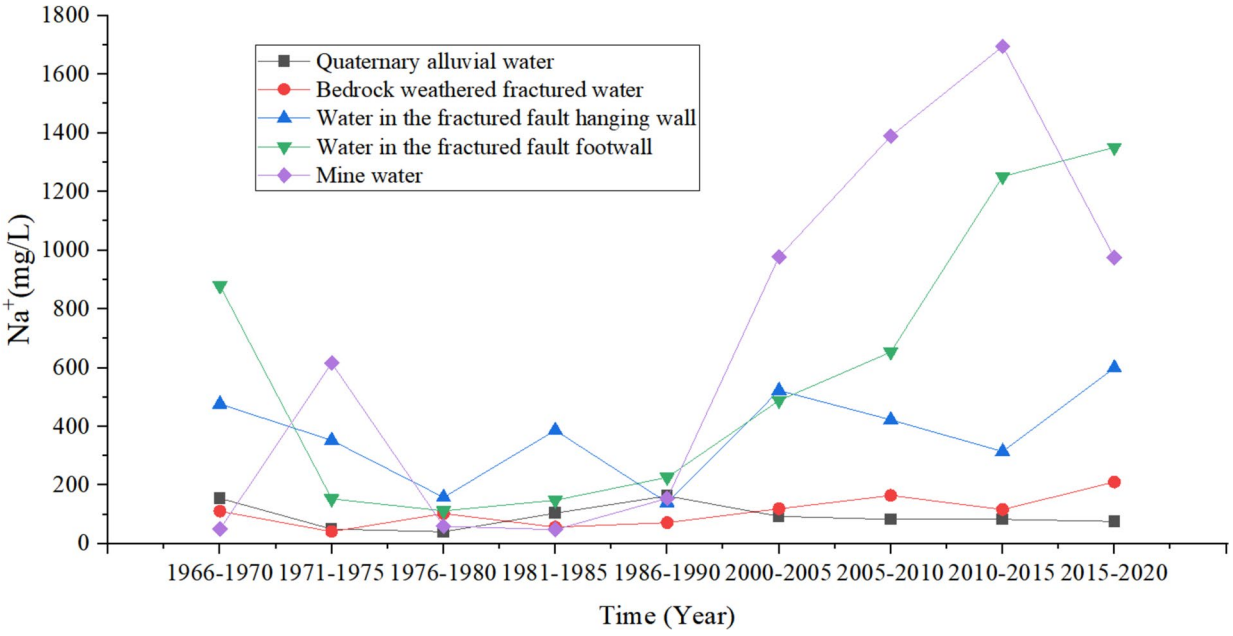

Fig. 11 Na^+ concentration curve of water samples changing with time

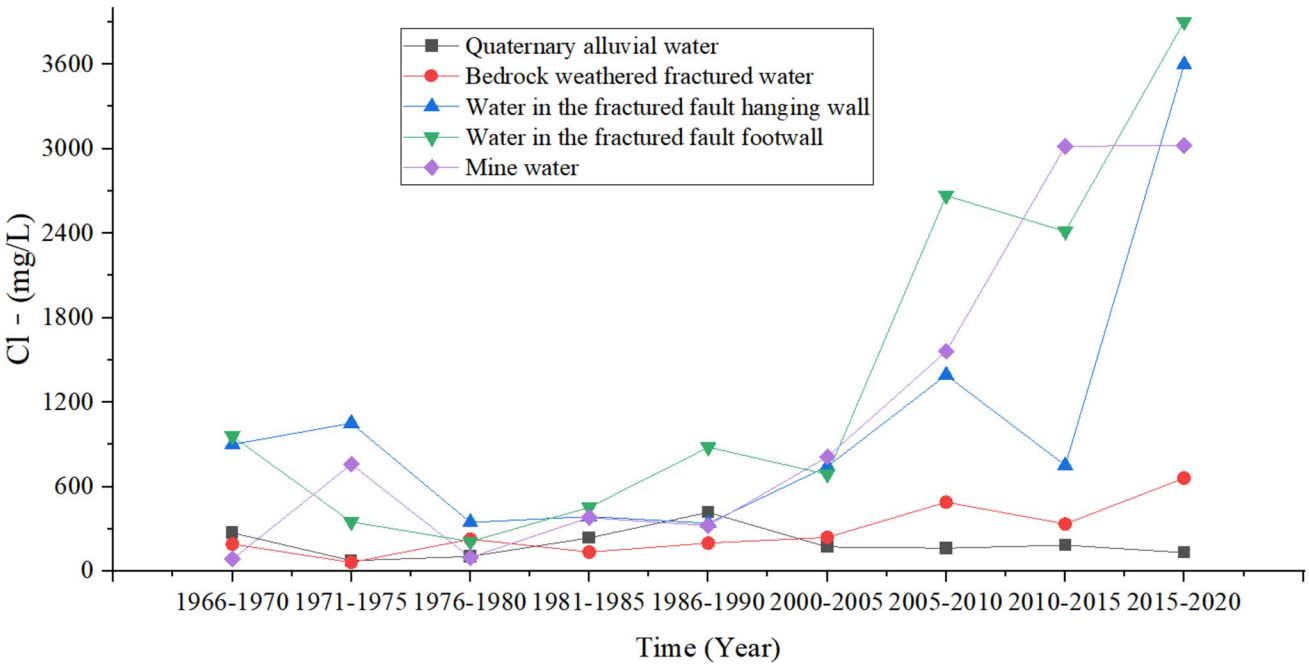

Fig. 12 Cl^- concentration curve of water samples changing with time

fault hanging wall, indicating close hydraulic connection between the fault hanging wall and footwall, and that the water in the fractured fault hanging wall had entered the stope through a water-conducting passageway.

Grey Correlation Analysis

Analytical Method

SAR, γNa/γCl, γMg/γCa, γCa/γNa, γMg/γNa, γCa/γCl,

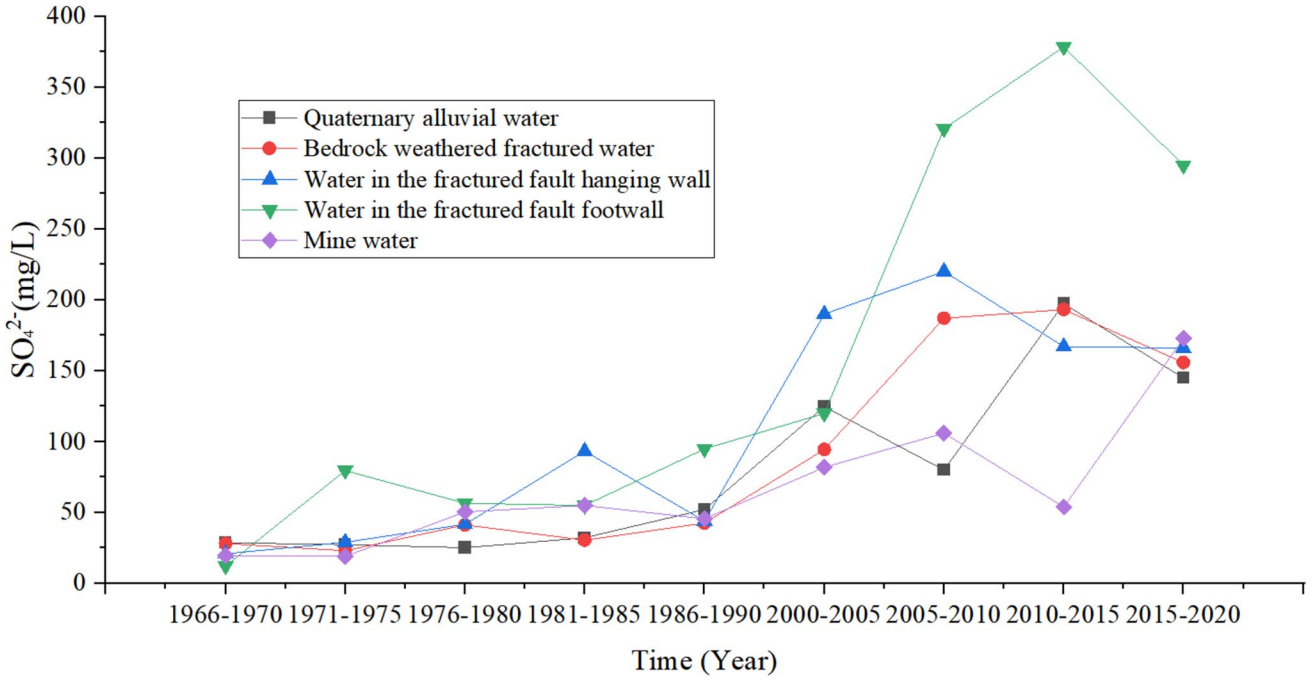

Fig. 13 SO_4^{2-} concentration curve of water samples changing with time

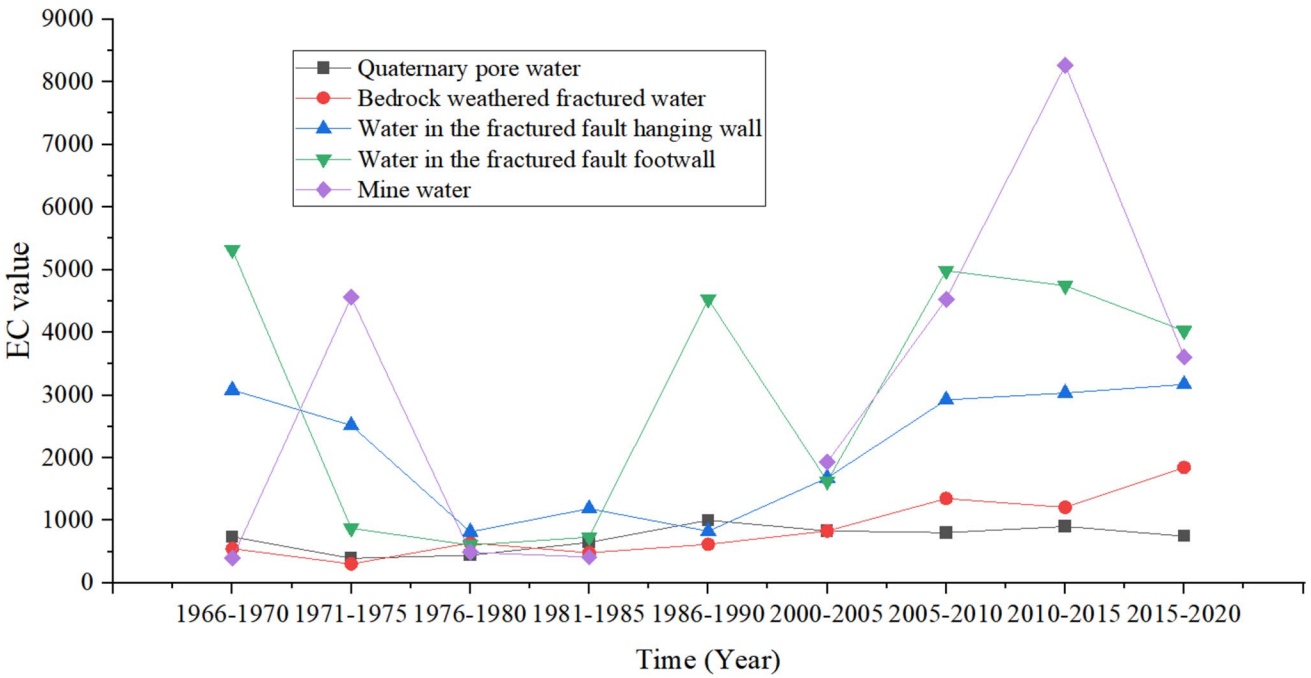

Fig. 14 EC value curve of water samples changing with time

$\gamma SO_4/\gamma Cl$, and $\gamma HCO_3/\gamma Cl$ were selected as components of the impact index, to analyze the source of the mine water and to determine the relationship between the mine water, various aquifers, and seawater. The correlation between the mine water samples and the water sample sequence of each water filling source was calculated by Deng's grey correlation method, which compares the degree of similarity between two sequences (Zhang and Yang 2018).

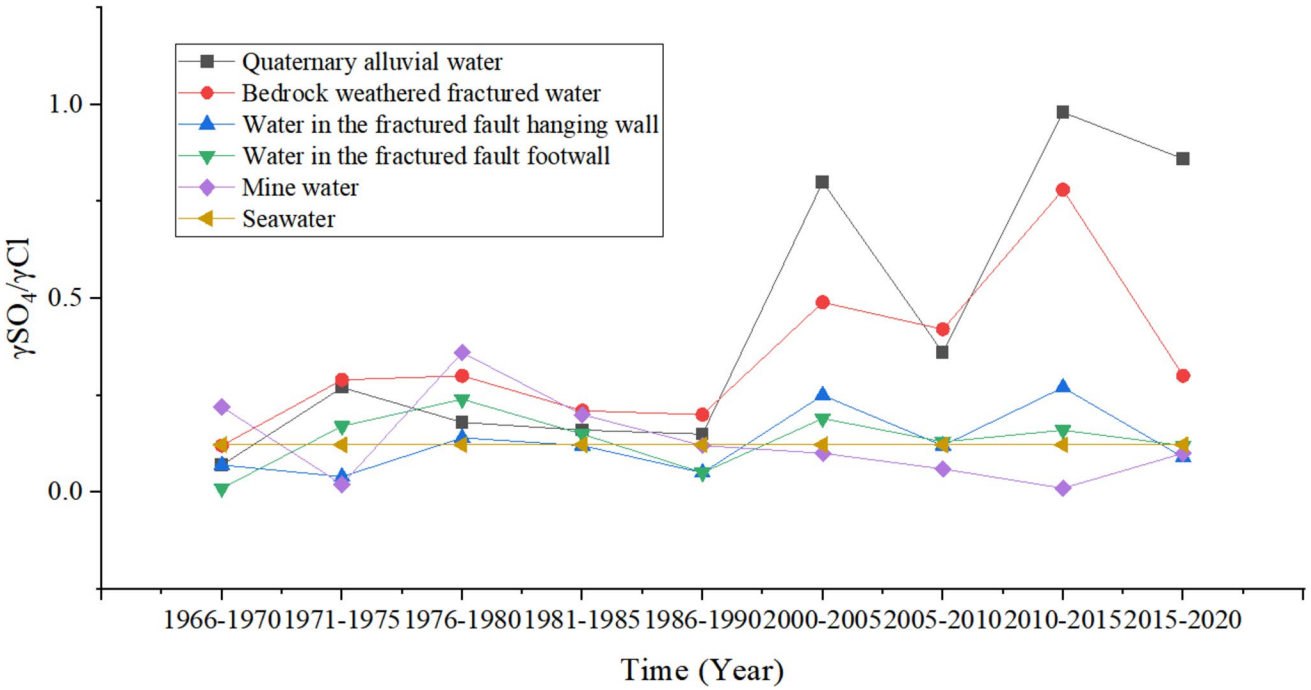

Fig. 15 γSO4/γCl curve of water samples changing with time

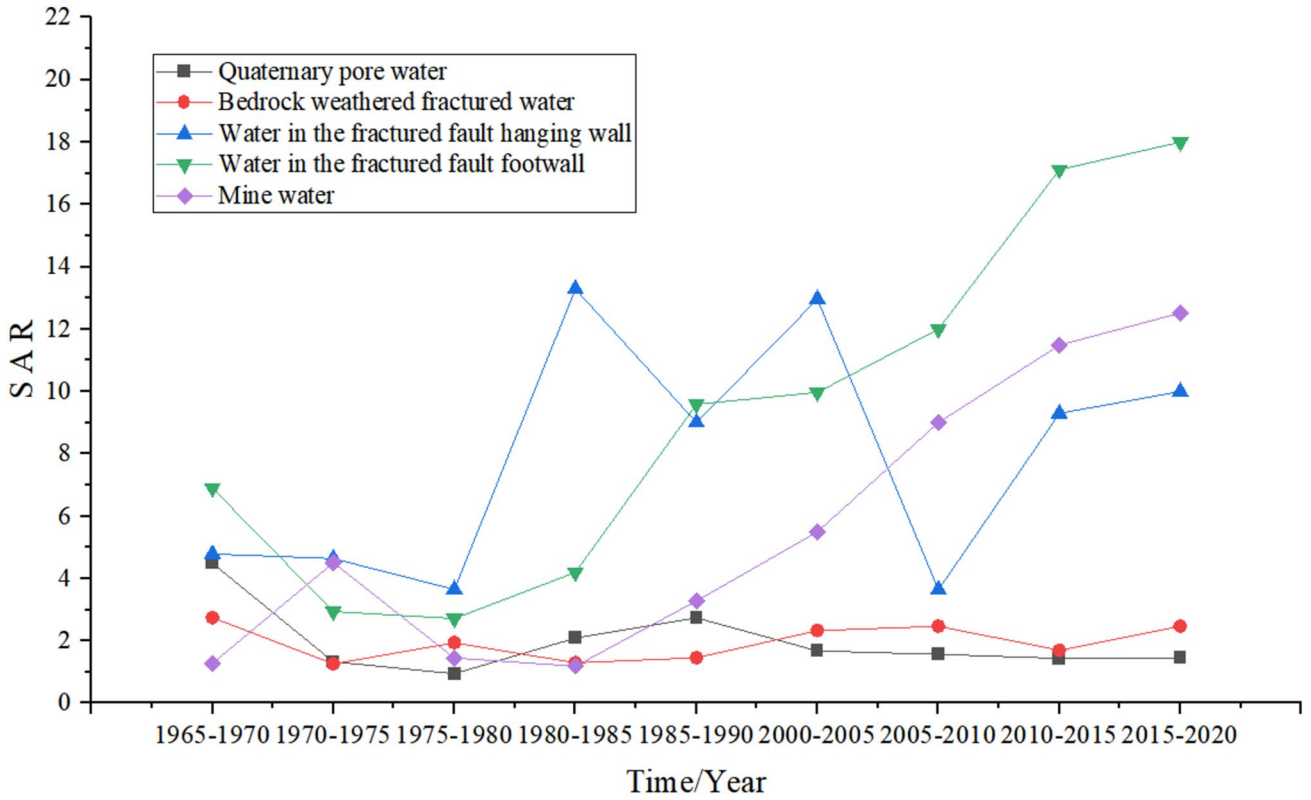

Fig. 16 SAR value curve of water samples changing with time

Analysis Results

We calculated the correlation between the mine water and samples of the water-filling sources using the MATLAB platform. The results are shown in Table 5.

Figure 17 shows that the greatest degree of correlation was between the mine water and the water in the fractured fault footwall, exceeding 0.9; the maximum value was the − 630 m mine water of the Xincheng gold mine (S1610580), which reached 0.93. This is because the no. 1 ore body is mainly distributed in the pyritic sericitized cataclastic rock belt, which is close to the main fault surface. So most of the mining was carried out in the fractured fault hanging wall a, which is the mine's direct aquifer. The correlation between the water samples in the fractured fault hanging wall and the mine water samples ranks second, with a range of 0.87–0.92 with a large value. This may be due to displacement and deformation of the overlying strata during mining, which opens the closed initial fissures to form water-conducting passageways leading to the mine.

The correlation between the bedrock weathered fracture water samples and mine water samples ranks third, all less

Table 5 Correlation degree between mine water and various water filling sources

Number	Sample number	Sampling location	Quaternary	Bedrock weathering	Fault hanging wall	Fault footwall	Seawater
1	S160501	Exploration roadway 1# of the Xincheng gold mine	0.826	0.872	0.896	0.925	0.829
2	S160502	Roadway 2# of the Xincheng gold mine	0.826	0.872	0.897	0.925	0.830
3	S160508	− 630 m middle section of Sizhuang gold mine	0.796	0.845	0.871	0.9	0.833
4	S160509	− 630 m middle section of Wangershan gold mine	0.825	0.876	0.9	0.927	0.823
5	S1610580	− 630 m mine water of Xincheng gold mine	0.834	0.886	0.908	0.933	0.822
6	S1610581	− 630 m observation point of Xincheng gold mine	0.834	0.881	0.906	0.932	0.826
7	J2013-630	Water inrush point of − 630 m roadway in the Jiaojia gold mine	0.808	0.862	0.877	0.921	0.817
8	J2013-330	Water inrush point of − 330 m roadway in the Jiaojia gold mine	0.845	0.894	0.915	0.932	0.803

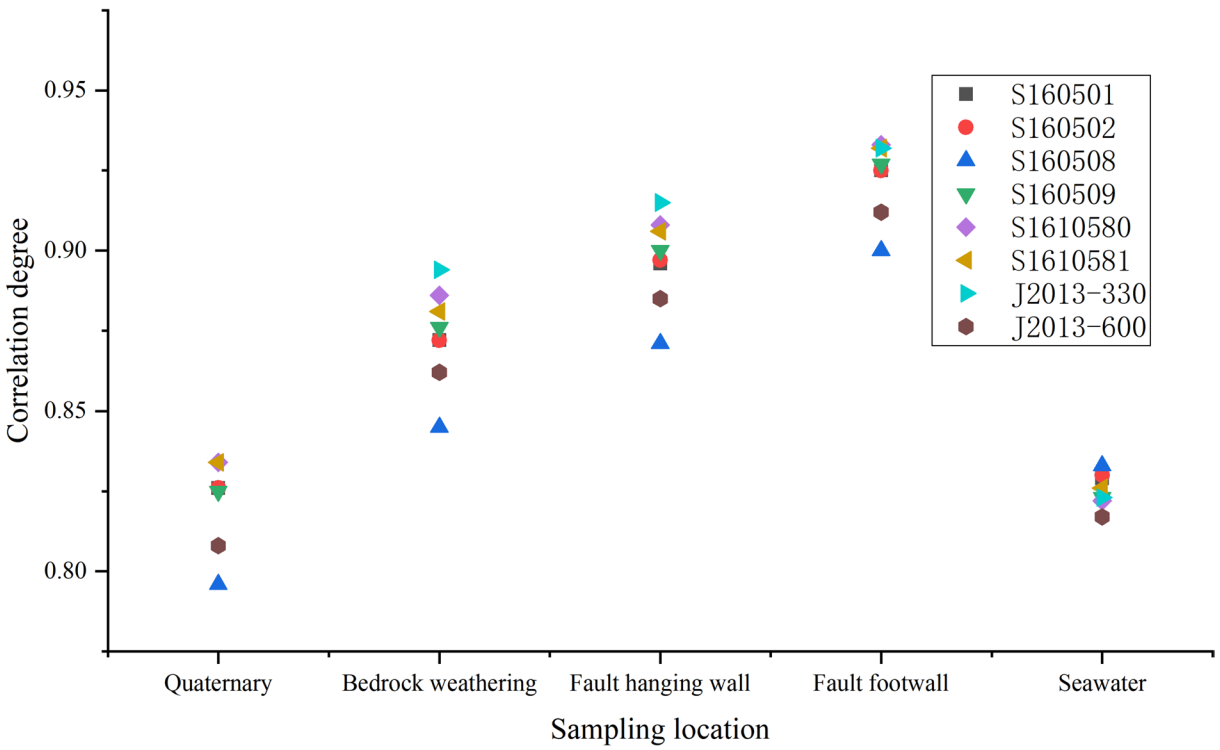

Fig. 17 Correlation degree between mine water and various water filling sources

than 0.9, with a range of 0.85–0.90, indicating a connection between the weathered fractured bedrock water and the mine water. This may be because some weathered fractured bedrock water enters the mine through the water-conducting passageway of the fault hanging wall or pre-existing fractures. The correlation between seawater samples and mine water samples ranks fourth, with a range of 0.80–0.833, indicating a possible connection between the mine water and seawater.

The correlation between the water inrush point at − 600 m mining level and seawater is greater than at the water inrush point at the − 300 m mining level, indicating that the connection between mine water and seawater increases with mining depth. The correlation between Quaternary alluvial water samples and mine water samples ranks fifth, indicating no connection between the two.

Discussion

With the increased mining depth, the chemical characteristics of the formation water in the mining area have changed significantly. Due to the different amounts of sulfur-bearing gold ore, iron ore, and marble in the Jiaojia mining area, mining activities were conducive to pyrite oxidation. Where carbonate rock or sulfate was present in the underground aquifer, the acidic groundwater would have accelerated the dissolution of carbonate rock or sulfate minerals, increasing the pH and the load of SO_4^{2-}, Ca^{2+}, and Mg^{2}.

The groundwater leaching effect was strong. As the groundwater containing Ca^{2+} and Mg^{2+} flows through the rock stratum, the cation exchange of Na^{+} and Ca^{2+} with Mg^{2+} occurs, increasing the Na^{+} load and decreasing the Ca^{2+} and Mg^{2+} load.

$$2Na^{+}(\text{Rock}) + Ca^{2+}(\text{Water}) \rightarrow 2Na^{+}(\text{Water}) + Ca^{2+}(\text{Rock}) \quad (2)$$

$$2Na^{+}(\text{Rock}) + Mg^{2+}(\text{Water}) \rightarrow 2Na^{+}(\text{Water}) + Mg^{2+}(\text{Rock}) \quad (3)$$

Due to the complex characteristics of groundwater migration, mixing, and diffusion processes, the evolution of groundwater chemical characteristics is affected by many factors with complicated and long-time processes. For example, under the influence of mining, hydrochemical reactions occurred after water mixed in the fractured fault hanging wall and footwall. Due to the greenhouse effect and other reasons, the sea level is rising, which increases the specific head height, and may intensify seawater intrusion. In addition, saltwater intrusion may be induced by mine dewatering or pumping of wells for non-mining uses. Due to the different geological structure properties and scale in the Jiaojia gold mine area, the faults may act as a barrier or water-conducting passageway in different regions. Generally, the reverse fault is compressed to form dense rock, which makes it easy to form a water barrier. The normal fault is stretched to form loose rock, which can form a water-conducting passageway. Therefore, the above-influencing factors should be added to future simulations or process experimental models to make the model more accurate.

Conclusion

The source of the mine water was analyzed by hydrochemical characteristics. According to the Piper diagram, analysis of the ion proportional coefficient, and grey correlation analysis, along with the relationship between water-filling source and mine water, the chemical characteristics and evolution of the groundwater were studied. The main conclusions are

(1) The main water inflow (inrush) source of the Jiaojia deep gold mine deep is the water in the fractured fault footwall, followed by the water in the fractured fault hanging wall. The bedrock water and Quaternary alluvial water are far from the gold deposit, making it difficult to enter the mine.
(2) Due to the influence of mining, the water in the fractured fault footwall enters the mine through the fracture near the Jiaojia main fault zone under the action of gravity, forming a close hydraulic connection with the water in the fractured fault footwall.
(3) With the increased mining depth, permeability pathways have formed between the seawater and mine water, and cation exchange reactions is becoming more intense. The water quality is becoming more saline and seawater infiltration has been enhanced.

Acknowledgements We gratefully acknowledge the financial support of the National Natural Science Foundation of China (Grant 42002282) and the Key Projects of the Shandong Natural Science Foundation (Grant ZR2020KE023).

References

Arefieva OD, Nazarkina AV, Gruschakova NV, Skurikhina JE, Kolycheva VB (2019) Impact of mine waters on chemical composition of soil in the Partizansk Coal Basin, Russia. ISWCR 7(1):7. https://doi.org/10.1016/j.iswcr.2019.01.001

Bayanzul B, Nakamura K, Machida I, Watanabe N, Komai T (2019) Construction of a conceptual model for confined groundwater flow in the Gunii Khooloi Basin, southern Gobi region, Mongolia. Hydrogeol J 27(5):1581–1596. https://doi.org/10.1007/s10040-019-01955-8

Chen K, Sun LH, Xu JY (2021) Statistical analyses of groundwater chemistry in the Qingdong coalmine, northern Anhui province, China implications for water–rock interaction and water source

identification. Appl Water Sci 11(2):50. https://doi.org/10.1007/s13201-021-01378-5
Erdogan IG, Fosso-Kankeu E, Ntwampe S, Ntwampe SKO, Waanders FB, Hoth N, Rand A (2019) Groundwater as an alternative source to irregular surface water in the O'Kiep area, Namaqualand, South Africa. Phys Chem Earth 114:102801. https://doi.org/10.1016/j.pce.2019.09.003
Farouk BA, Aubertin M, Simon R, Therrien R (2015) Numerical simulations of water flow and contaminants transport near mining wastes disposed in a fractured rock mass. Int J Min Sci Technol 25(1):37–45. https://doi.org/10.1016/j.ijmst.2014.11.003
Guiming D, Ying W, Juan T, Fan ZH (2021) Groundwater head uncertainty analysis in unsteady-state water flow models using the interval and perturbation methods. Hydrogeol J 29(5):1871–1883. https://doi.org/10.1007/s10040-021-02341-z
Herrera C, Godfrey L, Urrutia J, Custodio E, Jordan T, Jorge J, Delgado K, Barrenechea F (2022) Recharge and residence times of groundwater in hyper arid areas the confined aquifer of Calama, Loa River Basin, Atacama Desert. Chile. Sci Total Environ 752:141847. https://doi.org/10.1016/j.scitotenv.2020.141847
Irina T, Aleksei K, Alexander Z, Igor C (2022) Chemical composition of groundwater in abandoned coal mines evidence of hydrogeochemical evolution. Appl Geochem 137:105210. https://doi.org/10.1016/j.apgeochem.2022.105210
Khy EE, Toshifumi L, Megumi K, Tsurugi N, Carlito BT, Ryota F (2018) Groundwater monitoring of an open-pit limestone quarry Water-rock interaction and mixing estimation within the rock layers by geochemical and statistical analyses. Int J Min Sci Technol 28(6):849–857. https://doi.org/10.1016/j.ijmst.2018.04.002
Krzysztof C, Magdalena W, Agnieszka W, Christian W, Wojciech D, Dominika K, Danuta S (2021) Chemical variations in mine water of abandoned pyrite mines exemplified by the colorful lakes in Wieciszowice, Sudetes Mountains, Poland. J Hydrol 38:100974. https://doi.org/10.1016/j.ejrh.2021.100974
Liu J, Zhao Y, Tan T, Zhang S, Zhu F (2022) Evolution and modeling of mine water inflow and hazard characteristics in southern coalfields of China a case of Meitanba mine. Int J Min Sci Technol 32(3):12. https://doi.org/10.1016/j.ijmst.2022.04.001
Luo YJ, Ou LM, Chen JH, Gf Z, Xia YQ, Zhu BH, Zhou HY (2022) Hydration mechanisms of smithsonite from DFT-D calculations and MD simulations. Int J Min Sci Technol 32(3):605–613. https://doi.org/10.1016/j.ijmst.2022.01.009
Marion S, Georg W (2022) Closure of German hard coal mines effects and legal aspects of mine flooding. Mine Water Environ 41(1):280–291. https://doi.org/10.1007/s10230-021-00842-7
Ou S, Wang LG, Wang PP, Wang ZS, Huang JH, Zhou DL (2013) Numerical analysis of seepage flow characteristic of collapse column under the influence of mining. Int J Min Sci Technol 23(2):237–244. https://doi.org/10.1016/j.ijmst.2013.04.013
Paramaguru P, Chidambaram S, Pradeep K, Banajarani P, Devaraj N, Mahalakshmi M, Dhiraj KS, Meenu G, Ramanathan A (2021) Assessment and evaluation of geochemical process in the groundwater of the coastal aquifers. Acta Ecol Sin 2021:1872–2032. https://doi.org/10.1016/j.chnaes.2021.11.001
Pu L, Nils H, Carsten D, Liu P, Hoth N, Drebenstedt C, Sun YJ, Xu ZM et al (2017) Hydro-geochemical paths of multi-layer groundwater system in coal mining regions—using multivariate statistics and geochemical modeling approaches. Sci Total Environ 2017(601–602):1–14. https://doi.org/10.1016/j.scitotenv.2017.05.146
Sen W, Tiernan H, John M, Frank MD, Liam M (2021) Utilising CoDA methods for the spatio-temporal geochemical characterisation of groundwater; a case study from Lisheen Mine, south central Ireland. Appl Geochem 127:104912. https://doi.org/10.1016/j.apgeochem.2021.104912
Subodh CP, Abu R, Rabin C, Md SI, Asish S, Manisa S (2022) Application of data-mining technique and hydro-chemical data for evaluating vulnerability of groundwater in Indo-Gangetic Plain. J Environ Manage 318:115582. https://doi.org/10.1016/j.jenvman.2022.115582
Sunkari ED, Seidu J, Ewusi A (2022) Hydrogeochemical evolution and assessment of groundwater quality in the Togo and Dahomeyan aquifers, greater Accra region, Ghana. Environ Res 208:1–15. https://doi.org/10.1016/j.envres.2022.112679
Swa B, Tha B, Jma B et al (2021) Utilising CoDA methods for the spatio-temporal geochemical characterisation of groundwater; a case study from Lisheen Mine, south central Ireland. Appl Geochem 127:104912. https://doi.org/10.1016/j.apgeochem.2021.104912
Tarasenko I, Kholodov A, Zin'Kov A et al (2022) Chemical composition of groundwater in abandoned coal mines: evidence of hydrogeochemical evolution. Appl Geochem 137:105210. https://doi.org/10.1016/j.apgeochem.2022.105210
Weightman E, Craw D, Rufaut C, Kerr G, Scott J (2020) Chemical evolution and evaporation of shallow groundwaters discharging from a gold mine, southern New Zealand. Appl Geochem 122:104766. https://doi.org/10.1016/j.apgeochem.2020.104766
Yao BH, Bai HB, Zhang BY (2012) Numerical simulation on the risk of roof water inrush in the Wuyang coal mine. Int J Min Sci Technol 22(2):5. https://doi.org/10.1016/j.ijmst.2012.03.006
Zhang J, Yang T (2018) Study of a roof water inrush prediction model in shallow seam mining based on an analytic hierarchy process using a grey relational analysis method. Arab J Geosci 11(7):153. https://doi.org/10.1007/s12517-018-3498-2
Zhang K, Li HF, Han JM, Jiang BB, Gao J (2021) Understanding of mineral change mechanisms in coal mine groundwater reservoir and their influences on effluent water quality an experimental study. Int J Coal Sci Technol 8(1):14. https://doi.org/10.1007/s40789-020-00368-3
Zhou SH, Sun L, Shi ZM, Qu S, Bian MM, Yu DG, Singh VP (2022) Forecasting groundwater level of karst aquifer in a large mining area using partial mutual information and NARX hybrid model. Environ Res 213:113747. https://doi.org/10.1016/j.envres.2022.113747